A tumor-associated splice-isoform of *MAP2K7* drives dedifferentiation in MBNL1-low cancers via JNK activation

Debleena Ray[a,1], Yu Chye Yun[a], Muhammad Idris[a], Shanshan Cheng[a,b], Arnoud Boot[a,b], Tan Bee Huat Iain[c], Steven G. Rozen[a,b], Patrick Tan[a], and David M. Epstein[a,1]

[a]Cancer and Stem Cell Biology Program, Duke-NUS Medical School, 165897 Singapore, Singapore; [b]Centre for Computational Biology, Duke-NUS Medical School, 165897 Singapore, Singapore; and [c]Division of Medical Oncology, National Cancer Centre, 169610 Singapore, Singapore

Edited by James L. Manley, Columbia University, New York, NY, and approved May 28, 2020 (received for review February 11, 2020)

Master splicing regulator MBNL1 shapes large transcriptomic changes that drive cellular differentiation during development. Here we demonstrate that MBNL1 is a suppressor of tumor dedifferentiation. We surveyed *MBNL1* expression in matched tumor/normal pairs across The Cancer Genome Atlas and found that *MBNL1* was down-regulated in several common cancers. Down-regulation of *MBNL1* predicted poor overall survival in breast, lung, and stomach adenocarcinomas and increased relapse and distant metastasis in triple-negative breast cancer. Down-regulation of MBNL1 led to increased tumorigenic and stem/progenitor-like properties in vitro and in vivo. A discrete set of alternative splicing events (ASEs) are shared between *MBNL1*-low cancers and embryonic stem cells including a *MAP2K7*Δexon2 splice variant that leads to increased stem/progenitor-like properties via JNK activation. Accordingly, JNK inhibition is capable of reversing *MAP2K7*Δexon2-driven tumor dedifferentiation in MBNL1-low cancer cells. Our work elucidates an alternative-splicing mechanism that drives tumor dedifferentiation and identifies biomarkers that predict enhanced susceptibility to JNK inhibition.

MBNL1 | MAP2K7 | JNK inhibitors | alternative splicing | tumor cell dedifferentiation

Alternative splicing (AS) is a posttranscriptional mechanism that increases eukaryotic protein diversity during development (1). Consequently, AS results in acquisition of cellular and organ identity conferred by differential isoform profiles (2). As developmental growth signaling pathways are often coopted in cancer, aberrant AS is a hallmark of cancer progression and metastasis (3, 4). Specific tumor initiating cell (TIC) or cancer stem cell (CSC) populations are also known for specific splicing alterations in *CD44* or alpha6 integrin in breast (5, 6) and *DCLK1* in kidney cancer (7). Recently, TICs were reported to acquire resistance to immunotherapy in skin cancer models, placing TICs as the root cause of tumor relapse and an important therapeutic target (8).

At the cellular level, tumorigenic dedifferentiation results in acquisition of cellular plasticity, or stemness, that has many similarities with the pluripotent states of embryonic stem cells (ESCs) and induced pluripotent stem cells (iPSCs) (9). Profound splicing alterations occur during differentiation of stem and progenitor cells (10) as well as during somatic reprogramming of differentiated cells into iPSCs by the Yamanaka factors (11). In an effort to understand how AS profiles drive such dramatic cell fate changes, Han et al. compared AS patterns in ESCs and iPSCs with those of differentiated mouse and human cell types (12). Remarkably, they found that levels of muscleblind-like proteins (MBNL1 and MBNL2), implicated in myotonic dystrophy, not only differed between pluripotent (low) and differentiated (high) cells, but also controlled differentiation such that reducing MBNL1 and MBNL2 expression in differentiated cells led to a switch toward an ESC-like AS pattern and vice versa. This work demonstrated that MBNL proteins function as master splicing regulators capable of shaping large transcriptomic changes that can drive cellular differentiation.

Muscleblind-like 1 (MBNL1) is a C3H zinc-finger RNA-binding protein that is involved in multiple RNA-processing steps during development (13–16). *MBNL1*Δexon7 isoform functions as a tumor suppressor in prostate cancer (17) by regulating splicing and transcript abundance of genes involved in DNA repair, cell cycle, and migration. It also suppresses metastasis in breast (18) and colon cancer (19) by regulating transcript abundance of DBNL, TACC1, and SNAIL transcripts, respectively. MBNL1 has also been predicted to control AS patterns of undifferentiated cells across solid tumors (20), a finding that suggests that MBNL1-driven AS events might underlie emergence of TICs and tumor relapse. The extent to which MBNL1 functions to drive dedifferentiation and acquisition of stemness properties for the emergence of TICs as well as underlying biological mechanisms governing this dedifferentiation remains unknown.

Here we report that low *MBNL1* expression is a phenotype of many common solid cancers and that it is correlated with reduced overall survival, increased relapse, and distant metastasis. We demonstrate that MBNL1 drives cellular dedifferentiation in cancer by regulating the skipping of exon2 of *MAP2K7* via JNK activation. Importantly, our data show that *MBNL1* and *MAP2K7Δexon2* expression are biomarkers for increased cancer stemness and

Significance

Targeting stem-like cells in cancer is critical to overcoming resistance and relapse post chemotherapy or immunotherapy. We elucidate an alternative-splicing driven mechanism of cancer dedifferentiation and define a molecular context wherein stem-like tumor cells show enhanced susceptibility to JNK inhibition. MBNL1 and *MAP2K7*Δexon2 can prognosticate patients for JNK inhibition that can render stem-like tumor cells susceptible to therapy.

Author contributions: D.R. designed research; D.R., Y.C.Y., M.I., and S.C. performed research; T.B.H.I., S.G.R., P.T., and D.M.E. contributed new reagents/analytic tools; D.R., M.I., S.C., and A.B. analyzed data; D.R. wrote the paper; and D.M.E. provided overall supervision.

Competing interest statement: D.R is an inventor on a patent "Stratification of Cancer Patients by MBNL1 and MAP2K7Δexon2 Expression for Susceptibility to JNK Inhibition" filed in the Singapore patent office, Provisional Application No. 10201910208U. D.M.E is the founder, director, and CEO of Black Diamond Therapeutics and a consultant to Engine Bioscience in areas unrelated to this manuscript.

This article is a PNAS Direct Submission.

Data deposition: All RNA-seq data generated are available via European Nucleotide Archive (ENA) under accession no. PRJEB32567.

[1]To whom correspondence may be addressed. Email: debleena.ray@duke-nus.edu.sg or david.epstein@duke-nus.edu.sg.

This article contains supporting information online at https://www.pnas.org/lookup/suppl/doi:10.1073/pnas.2002499117/-/DCSupplemental.

First published June 29, 2020.

increased JNK activity. MBNL1–JNK-driven cancer stemness can be reversed by JNK inhibition.

Results

Down-Regulation of *MBNL1* Is Correlated with Poor Prognosis in Cancer. To survey *MBNL1* expression across different forms of cancer, we took advantage of The Cancer Genome Atlas (TCGA) from which RNA-sequencing (RNA-seq) data in 16 cancer types with matching tumor and normal samples were available. We found that *MBNL1* was significantly down-regulated in 8 cancer types—bladder, breast, colon, lung adenocarcinoma (LUAD), lung squamous cell carcinoma (LUSC), prostate, stomach, and uterine cancers—which we hereafter refer to as *MBNL1*-low cancers. *MBNL1* was also up-regulated in three subtypes of renal cancer (Fig. 1*A* and Dataset S1, Table S1). In total, 312 (86%) tumors out of 360 analyzed tumor/normal pairs across the "*MBNL1*-low cancers" show lower expression of *MBNL1* (Fig. 1*B*). As MBNL1 and MBNL2 share structural and functional similarities (21), we analyzed the expression of *MBNL2* using the same TCGA RNA-seq data. *MBNL2* was down-regulated in all *MBNL1*-low cancers except for colon adenocarcinoma (COAD) (*SI Appendix*, Fig. S1*A* and Dataset S1, Table S1), indicating a complementary role for MBNL1 and 2 in most MBNL1-low cancers.

We next performed immunohistochemistry (IHC) in an independent cohort of matched stomach adenocarcinoma clinical samples and found that MBNL1 was down-regulated in 36% of those samples (9/25) (Fig. 1*C*, *SI Appendix*, Fig. S1 *B* and *C*, and Dataset S1, Table S2). MBNL1 showed both nuclear and

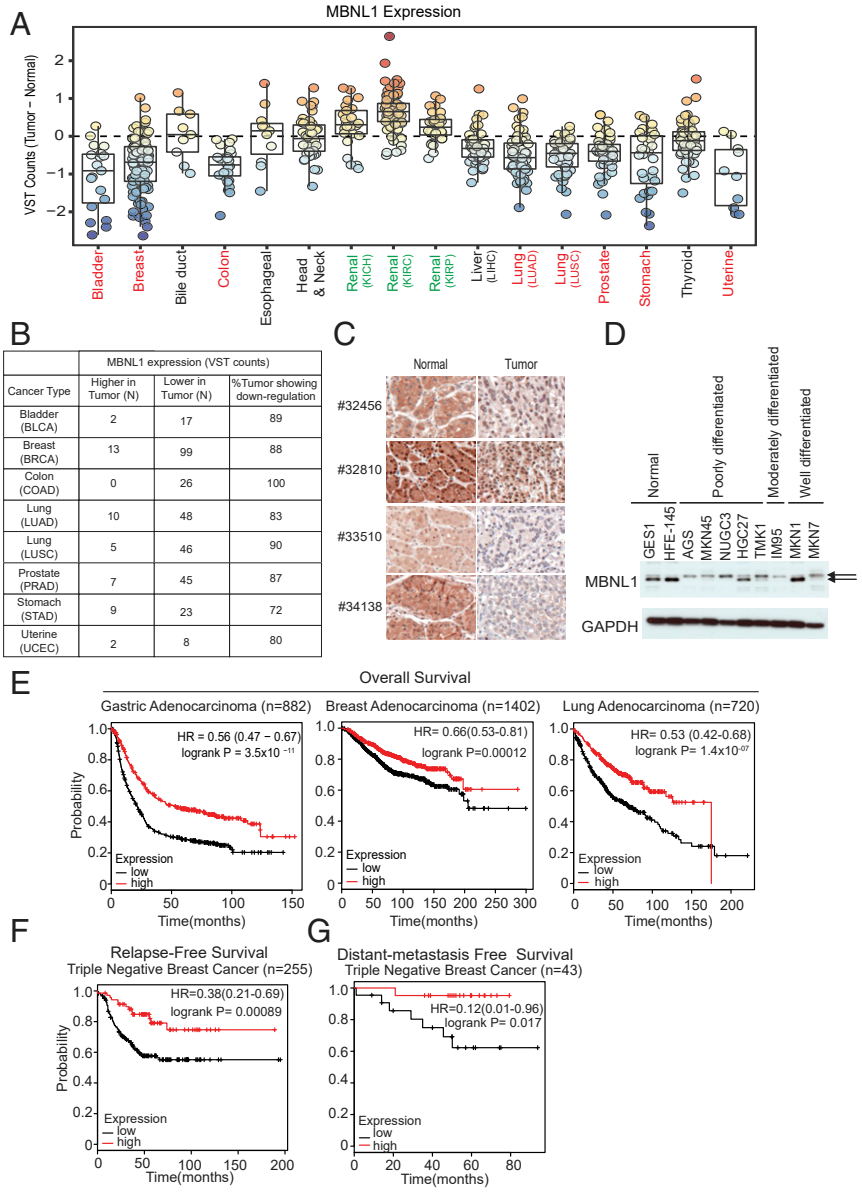

	MBNL1 expression (VST counts)		
Cancer Type	Higher in Tumor (N)	Lower in Tumor (N)	%Tumor showing down-regulation
Bladder (BLCA)	2	17	89
Breast (BRCA)	13	99	88
Colon (COAD)	0	26	100
Lung (LUAD)	10	48	83
Lung (LUSC)	5	46	90
Prostate (PRAD)	7	45	87
Stomach (STAD)	9	23	72
Uterine (UCEC)	2	8	80

Fig. 1. *MBNL1* is down-regulated in cancer and is a prognostic marker for survival. (*A*) Box plot showing median difference in variance stabilized transformed read counts (VST counts) for *MBNL1*. Each shaded circle (red, up-regulated; blue, down-regulated) represents a unique patient. Down-regulated indicated in red font, up-regulated by green font (log2 fold change >0.5 (abs), *P* value <0.05) and no change in black font. (*B*) The table lists number (N) of patients with higher or lower MBNL1 expression in matched tumors/normal. (*C*) Representative MBNL1 expression (IHC) in matched tumor and normal stomach adenocarcinoma patients in a tissue microarray (TMA). (*D*) Western blot showing MBNL1 expression. (*E*) Kaplan–Meier plots showing correlation between *MBNL1* and overall survival. (*F* and *G*) Kaplan–Meier plots showing correlation between MBNL1 expression and "relapse-free survival" and "distant-metastasis-free survival."

cytoplasmic staining as previously reported (22). As MBNL1 is ubiquitously expressed, we used excised MBNL1 knockdown (KD) MDA-MB-231 xenograft tumors as a negative control for our MBNL1 antibody in IHC (see Fig. 3*E*). Western blot showed MBNL1 is down-regulated in six poor-to-moderately differentiated stomach cancer cell lines and not in two well-differentiated stomach cancer cell lines as compared to GES-1 and HFE-145, non-neoplastic gastric epithelial cell lines (Fig. 1*D*, *SI Appendix*, Fig. S1*D*, and Dataset S1, Table S3). We note that several stomach cancer cell lines in Fig. 1*D* express the exon5^{+} *MBNL1* isoform identified by RT-PCR (*SI Appendix*, Fig. S1*E*). This is a recurrent tumor-associated splice isoform in colorectal, lung, and breast tumors (23). The inclusion of exon5 is driven by down-regulation of MBNL1 protein (24). This isoform is distinct from that described in ref. 17. The specific function of exon5^{+} MBNL1 isoform in cancer is a current subject of research in our laboratory. Taken together, our data demonstrate that MBNL1 is consistently down-regulated across many cancers.

To understand the clinical significance of *MBNL1* down-regulation, we used a survival analysis tool called the Kaplan–Meier plotter (https://kmplot.com/analysis/). We found that low *MBNL1* expression was significantly correlated with poor overall survival in patients with stomach, breast, and lung adenocarcinomas (Fig. 1*E*). In triple-negative breast cancer (TNBC), a highly aggressive form of breast cancer associated with a high risk of relapse, low *MBNL1* expression correlated with increased relapse and distant metastasis (Fig. 1 *F* and *G*). We further validated this observation in two additional breast adenocarcinoma datasets: METABRIC (25) and data from Forero et al. (26). In the METABRIC cohort, low MBNL1 expression was significantly associated with poor overall survival (in ER^{-}/HER2^{-} and subtype agnostic, *SI Appendix*, Fig. S1 *F* and *G*). In

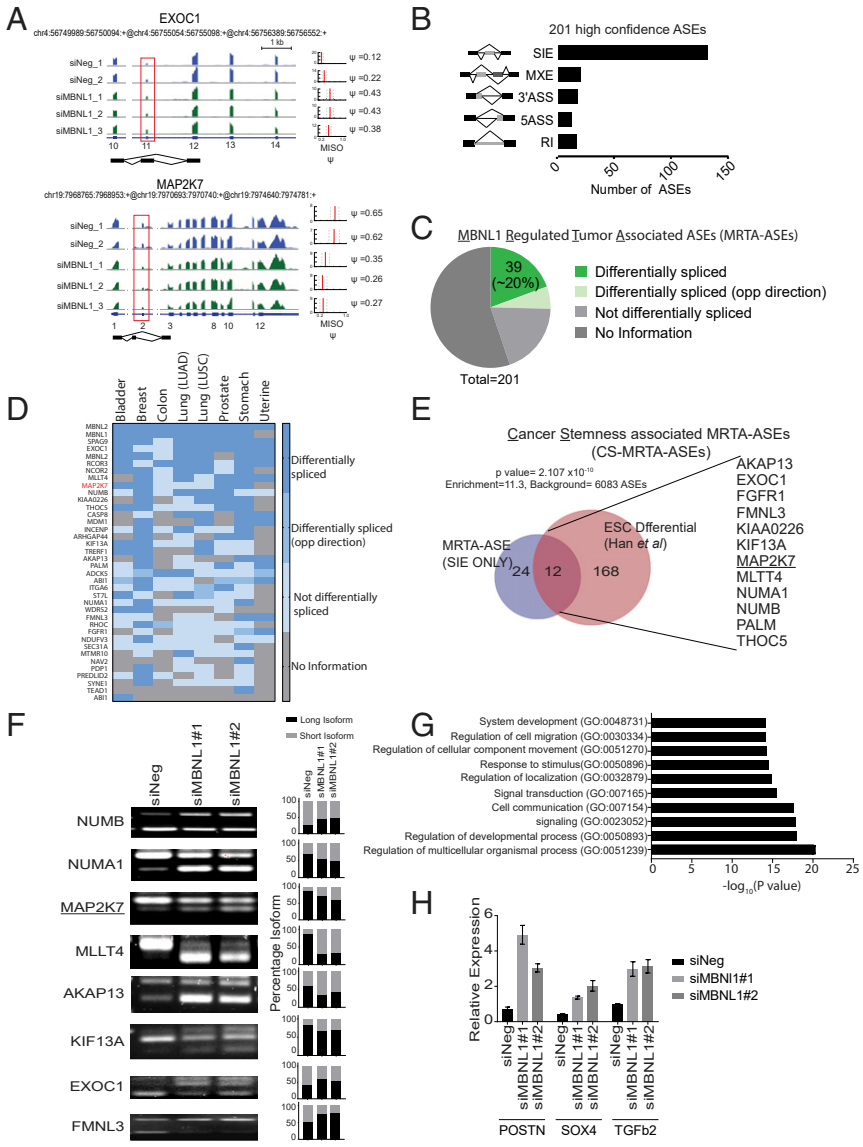

Fig. 2. MBNL1 KD up-regulates CSC-specific splice isoforms and genes. (*A*) Wiggle plots representing an inclusion event (*EXOC1*) and a skip event (*MAP2K7*). Histograms at *Right* show PSI values. (*B*) Quantification of different classes of high-confidence ASEs. (*C*) Pie chart showing high-confidence ASEs that are also differentially spliced in *MBNL1*-low cancers. (*D*) Qualitative heat map showing distribution of MRTA-ASEs. (*E*) Venn diagram showing overlap between the SIE events of MRTA-ASEs and ESC-differential ASEs from Han et al. (12). (*F*) Gel electrophoresis images (*Left*) and quantitative bar graphs (*Right*) showing validation of CS-MRTA-ASEs. (*G*) Bar graph showing biological processes GO term enrichment upon MBNL1 knockdown. (*H*) Validation of up-regulation of CSC-associated genes upon MBNL1 knockdown using two independent siRNAs by qRT-PCR. Data show mean ± SD.

the Forero et al. TNBC cohort (26), low expression of *MBNL1* was associated with increased relapse (note due to the small size of this cohort, $n = 38$, survival disadvantage is not statistically significant, $P = 0.0589$; *SI Appendix*, Fig. S1*H*). We further investigated genomic alterations at the *MBNL1* locus and their implications on clinical outcome. We found *MBNL1* genomic alterations are rare in MBNL1-low cancers (*SI Appendix*, Fig. S1 *I* and *J* and *SI Appendix*). Taken together, these data indicate that low *MBNL1* expression segregates with poor prognosis for some cancers.

Loss of MBNL1 Mediates Transcriptomic Alterations Associated with Stemness. To understand how MBNL1 down-regulation impacts transcriptomic changes, we performed RNA-seq upon knockdown of MBNL1 (using siRNA pool) in immortalized non-neoplastic stomach cell line HFE-145 (*SI Appendix*, Fig. S2*A*). We obtained 10^8 paired-end reads per sample and analyzed the data using the mixture-of-isoforms (MISO) pipeline to identify differentially spliced isoforms in control-KD pairs (27). We identified 926 differentially spliced alternative splicing events (ASEs) out of which 201 high-confidence ASEs that occur in four out of six replicate pairs and show greater than 20% difference in percent spliced in (PSI or ψ) values were identified (Dataset S1, Table S4). Wiggle plots demonstrating two high-confidence ASEs are shown as examples in Fig. 2*A* and *SI Appendix*, Fig. S2*D*. The high-confidence ASEs consisted of 132 skip-inclusion events (SIE), 21 mutually exclusive events (MXE), 18 3′-alternative splice site selection events (3′ASS), 13 5′ASS events, and 17 retained intron (RI) events (Fig. 2*B* and Dataset S1, Table S4).

We next asked whether the high-confidence ASEs we identified in HFE-145 cells were also differentially spliced in *MBNL1*-low cancers. To answer this question we interrogated the PSI values of high-confidence ASEs (downloaded from https://bioinformatics.mdanderson.org/TCGASpliceSeq) in matched tumor–normal samples in bladder, breast, colon, lung (LUAD and LUSC), prostate, stomach, and uterine cancers from the TCGA RNA-seq data. We found that 39 of the 201 (~20%) high-confidence ASEs, in at least one *MBNL1*-low cancer showed statistically significant difference in median PSI value between tumor and normal samples (P value <0.05, determined by Wilcoxon signed-rank test) in the direction concordant with KD of MBNL1 in HFE-145 cells (Fig. 2 *C* and *D*). We defined this subset of 39 ASEs as "MBNL1-regulated tumor-associated ASEs" (MRTA-ASEs) (Dataset S1, Table S5 and Fig. 2 *C* and *D*). Interestingly COAD shows the least number of MRTA-ASEs (Fig. 2*D*) despite showing down-regulation of *MBNL1* in 100% of tumors (Fig. 1 *A* and *B*). It is noteworthy that COAD is also the only *MBNL1*-low cancer that does not present down-regulation of *MBNL2* (*SI Appendix*, Fig. S1*A*). Therefore, this lack of MRTA-ASEs might be attributed to the compensatory role of *MBNL2* (21).

Corollary to this analysis, we compared the high-confidence ASEs with *MBNL1* correlated tumor-associated (TA)-ASEs computed by Sebestyén et al. and Cheng et al. (20, 28). We found 17 overlapping ASEs between our high-confidence ASEs and MBNL1-correlated TA-ASEs from the above studies (Dataset S1, Table S6). These 17 *MBNL1*-correlated TA-ASEs showed a very significant overlap with MRTA-ASEs (P value = 2.874×10^{-8} and an enrichment of 9.7-fold over any overlap occurring by chance, *SI Appendix*, Fig. S2*B* and Dataset S1, Table S6).

MRTA-ASEs include ASEs in *MBNL1* itself and in *MBNL2*, indicating self-regulation as previously reported (24). They further include ASEs of cytoskeletal genes involved in epithelial–mesenchymal transition (e.g., *FMNL3*), transcription and chromatin remodeling genes (e.g., *TRERF1*, *NCOR3*, *RCOR3*, and *TEAD1*), cell cycle and cell division genes (e.g., *KIF13A*, *NUMA1*, and *SYNE1*), and JNK signaling pathway genes (e.g., *MAP2K7* and *SPAG9*). Gene Ontology (GO) term analysis of *MBNL1* correlated TA-ASEs in MBNL1-low cancers from Sebestyén et al. (20) showed the enrichment of "actin cytoskeleton organization" GO: 0030036 (P value = 4.38×10^{-06}) as the key biological process enriched. Our previous work also showed that MBNL1 is one of the key splice factors that regulate an AS program in gastric cancer involved in actin cytoskeleton reorganization associated with invasive/metastatic properties of cancer (28). Together, this suggests that MBNL1 down-regulation-mediated AS affects important cellular processes involved in cancer.

Han et al. reported that different AS patterns between ESCs and differentiated cells are controlled by MBNL proteins (12). An ESC-specific switch in FOXP1 controls dedifferentiation of differentiated cells into ESC-like cells. They also found that MBNL proteins are expressed at low levels in ESCs, and that MBNL1 and MBNL2 KD in mouse embryonic fibroblasts enhance somatic reprogramming efficiency by the Yamanaka "OKSM" factors (12). To explore whether any of the MRTA-ASEs was present in the Han et al. dataset, we compared the overlap between the SIEs from our MRTA-ASEs with the ESC-differential SIEs defined by Han et al. We discovered that there were indeed 12 overlapping ASEs (P value = 2.107×10^{-10} and an enrichment of 11.3-fold over any overlap expected by chance), and that for each of them the direction of splicing in cancer is toward ESCs (Fig. 2*E* and Dataset S1, Table S7). We defined these 12 ASEs as cancer stemness-associated MRTA-ASEs (CS-MRTA-ASEs). We validated 8 out of the 12 CS-MRTA-ASEs by RT-PCR in MBNL1 KD HFE-145 cells using two separate siRNAs (Fig. 2*F*). Two out of the remaining 4 CS-MRTA-ASEs did not show differential splicing while for the other two, we failed to design a sufficiently specific primer set. Importantly, CS-MRTA-ASEs include two known oncogenic ASEs: *NUMB* (29) and *NUMA1* (20). However, in our dataset we did not observe any differential splicing alterations in *FOXP1*, identified by Han et al. (12), as the primary ASE that drives dedifferentiation. We further surveyed the TCGA RNA-seq data and discovered that *FOXP1* was not differentially spliced between tumor and normal in any of the *MBNL1*-low cancers, indicating that FOXP1 isoforms do not play a role in tumor dedifferentiation (*SI Appendix*, Fig. S2*C*).

Along with splicing, MBNL1 affects transcript stability (15). We therefore analyzed the effect of MBNL1 KD on gene expression changes. We identified 1,630 up-regulated and 1,341 down-regulated genes in MBNL1 KD HFE-145 cells (Dataset S1, Table S8). Gene ontology analysis (PANTHER overrepresentation test, (*SI Appendix*, *Materials and Methods*) shows that dysregulated genes regulate "developmental processes" (GO: 0050793) and "cell migration" (GO: 00303341, Fig. 2*G* and Dataset S1, Table S9). Up-regulated genes included *POSTN*, *TGFb2*, *NOTCH3*, and *SOX4* that have established roles in CSC biology (30–32). We validated the up-regulation of these genes via qRT-PCR in MBNL1 KD HFE-145 cell lines using two separate siRNAs (Fig. 2*H*). Taken together, our data show that loss of MBNL1 in cancer up-regulates cancer stem cell-specific isoforms and transcripts associated with stem-like features. We therefore hypothesized: MBNL1 down-regulation drives tumorigenic dedifferentiation in cancer.

MBNL1 KD Increases Tumorigenic Properties in Normal and Cancer Cell Lines. Because increased clonogenic activity, migration, and invasion are functional properties adopted by undifferentiated cancer stem-like cells, we investigated such properties in vitro in stomach (AGS) and breast (MDA-MB-231) cancer cell lines as representative cellular models of *MBNL1*-low cancer and HFE-145 as a model for non-neoplastic epithelial cells. To this end, we generated stable MBNL1 knockdowns using two different shRNAs targeting constitutive exons of *MBNL1* and a non-targeting control shRNA (shNeg) (*Materials and Methods* and Fig. 3*A*). All MBNL1 KD cell lines showed increased soft-agar

colony formation (Fig. 3*B*) and increased in vitro cell migration (Fig. 3*D*) and invasion (*SI Appendix*, Fig. S3 *A* and *B*).

Importantly, subcutaneous (s.c.) cell injection into the flanks of nonobese diabetic/severe combined immunodeficient (NOD/SCID) mice ($n = 5$ per group) led to formation of larger tumors in mice that had received MBNL1 KD MDA-MB-231 cells compared to control cells (Fig. 3 *C* and *E*). Excised tumors were stained for MBNL1 expression using IHC to confirm sustained KD of MBNL1 (Fig. 3 *E*, *Right*). These data demonstrate that lowering MBNL1 expression increases in vitro and in vivo tumorigenic properties.

Low MBNL1 Expression Increases Stem/Progenitor-Like Properties in Cancer. We next focused our efforts on assessing self-renewal and long-term growth potential in vitro and in vivo as readouts of stem/progenitor-like functional properties in cancer cells. We found that larger and increased numbers of tumor spheres were formed upon KD of MBNL1 in limiting dilution assays in AGS and MDA-MB-231 cells (*SI Appendix*, Fig. S4 *A* and *B*). In serial replating assays, MBNL1 KD AGS cells were able to form tertiary spheroids unlike control cells, while MBNL1 KD MDA-MB-231 cells formed twice the number of tertiary spheroids relative to control cells (Fig. 4 *A* and *B*). S.c. injection of 4×10^6, 4×10^5, 4×10^4, and 4×10^3 MBNL1 KD and control MDA-MB-231 cells into the flanks of NOD/SCID mice ($n = 5$ per group) showed early tumor initiation and faster tumor growth at all cell dilutions. A total of 4,000 parental MDA-MB-231 cells injected into NOD/SCID mice completely failed to form any tumor, while 4,000 MBNL1 KD MDA-MB-231 cells showed tumor initiation in 2/5 mice 29 d postinjection (Fig. 4*C*). We also found that KD of MBNL1 led to the up-regulation of known CSC (*CD133* and *LGR5*) and pluripotency markers (*OCT4*, *NANOG*, and *SOX2*) in MDA-MB-231 and AGS cells (Fig. 4*D*).

To gain a deeper insight into stem-associated gene expression patterns resulting from low *MBNL1* expression in cancer, we scored tumor/normal pairs within TCGA stomach and breast cancer cohorts using defined ESC gene sets reported to be present in various forms of cancers (33). Correlation analysis between *MBNL1* expression and "stemness score" for each patient showed that lower *MBNL1* expression correlated with higher stemness gene expression pattern in these tumors. (Fig. 4*E*). This correlation is most prominent with wide confidence intervals in triple-negative breast cancer (Fig. 4*F*, however we note the low number of triple-negative samples in this TCGA cohort, $n = 11$ and a P value that was >0.05), which also shows increased relapse and distant metastasis as a function of *MBNL1* down-regulation (Fig. 1 *F* and *G*).

Finally, we grew parental MDA-MB231 and AGS cell lines as monolayers or as tumor spheroids in suspension to enrich for CSCs (ref. 34 and *SI Appendix*, Fig. S4 *C* and *D*) and measured MBNL1 expression by Western blot. Both AGS and MDA-MB-231 cells grown as tumor spheroids showed decreased MBNL1 expression relative to monolayer culture (Fig. 4*G*), indicating that low expression of MBNL1 marks stem/progenitor-like cells. Taken together, our data show that stem cell-like functional properties increase in cancers that present low expression of *MBNL1*.

MBNL1 Regulates Skipping of Exon2 of *MAP2K7* in Cancer. The 12 CS-MRTA-ASEs identified by us points to mechanisms by which MBNL1 might regulate acquisition of stem cell-like properties in cancer cells (Dataset S1, Table S7). We were intrigued to see the *MAP2K7*Δexon2 isoform in this subset, as this isoform is known to harbor a high-affinity JNK docking site (ref. 35 and *SI Appendix*, Fig. S5*A*) leading to activation of JNK signaling (36). Indeed, many studies have linked activated JNK with cancer stemness (37, 38), but more importantly, the MAP2K7/JNK pathway is druggable with existing small molecule and peptide inhibitors.

We found that knockdown of MBNL1 led to skipping of exon2 of *MAP2K7* in HFE-145 cells (Fig. 2 *E* and *F*). We validated this in stable MBNL1 KD MDA-MB-231 cells (Fig. 5*A*). Intronic region upstream and downstream of the skipped *MAP2K7* exon2 was enriched with statistically significant MBNL1 binding motifs: "*gcuugc*" (39) and "*ygcuky*" (40) (*SI Appendix*, Fig. S5 *B* and *C*). We further discovered that exon2 of *MAP2K7* is significantly skipped in many MBNL1-low cancers (i.e., bladder, breast, colon, prostate, and stomach, Fig. 5*B*). Spearman's correlation analysis showed that inclusion of exon2 of *MAP2K7* is inversely correlated with *MBNL1* expression in bladder, breast, prostate,

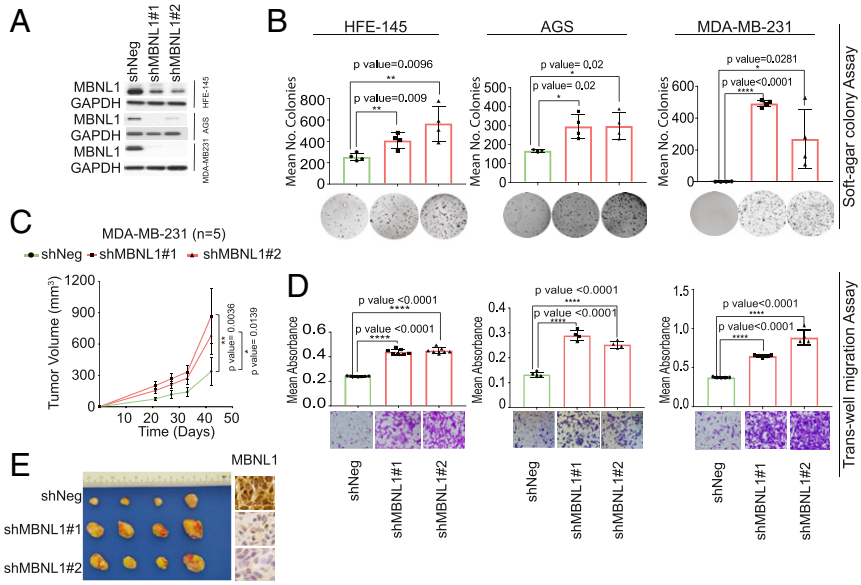

Fig. 3. MBNL1 KD increases in vitro colony formation, migration, and in vivo tumor formation. (*A*) Western blot showing expression of MBNL1 in indicated cell lines treated with nontargeting shRNA (shNeg) or two MBNL1 shRNAs. (*B* and *D*) Bar graphs (*Top*) and representative images (*Bottom*) showing soft agar colony formation (*B*) and in vitro Transwell migration (*D*) in indicated cell lines. Data show mean ± SD. See also *SI Appendix*, Fig. S3. (*C*) X-Y graph showing mean ± SD tumor volume (mm3) over time (days) in NOD/SCID mice injected with MDA-MB-231 cells treated with shNeg control shRNA (green) vs. MBNL1 KD cells (red). (*E*, *Left*) Image of resected tumors from four replicate mice per treatment category and IHC staining with MBNL1 primary antibody (*E*, *Right*) of the excised tumors.

and stomach cancers (Fig. 5*C*). We also discovered that (similar to down-regulation of *MBNL1* expression) increased skipping of *MAP2K7* exon2 correlated with a higher stemness score in stomach and breast cancer (Fig. 5*D*).

Low Levels of MBNL1 Activate JNK and Promote Acquisition of Stem Cell-Like Functional Properties by Alternative Splicing of *MAP2K7* Exon2. We next investigated how MBNL1 down-regulation and consequent up-regulation of *MAP2K7*Δexon2 splice isoform affects JNK activation, CSC and pluripotency marker expression, and in vitro migratory and invasive behavior. We observed that serum stimulation increased phospho JNK and phospho c-JUN in MBNL1 KD MDA-MB-231 and HFE-145 cells compared to cells transfected with control shRNA or siRNA, respectively (Fig. 6*A*). KD of MBNL1 in HFE-145 also led to up-regulation of CSC and pluripotency genes, except for *OCT4* (*SI Appendix*, Fig. S6*A*). We next used a panel of naturally MBNL1-low/*MAP2K7Δexon2*-high and MBNL1-high/*MAP2K7Δexon2*-low cancer cell lines (*SI Appendix*, Fig. S6 *B–E*) to analyze JNK signaling. Overall, MBNL1-low/*MAP2K7Δexon2*-high cell lines showed increased JNK activation upon serum stimulation compared to the MBNL1-high/*MAP2K7Δexon2*-low cell lines (Fig. 6 *B* and *C*). IM95 harbors an inactivating *MAP2K7* mutation (41); consequently, it

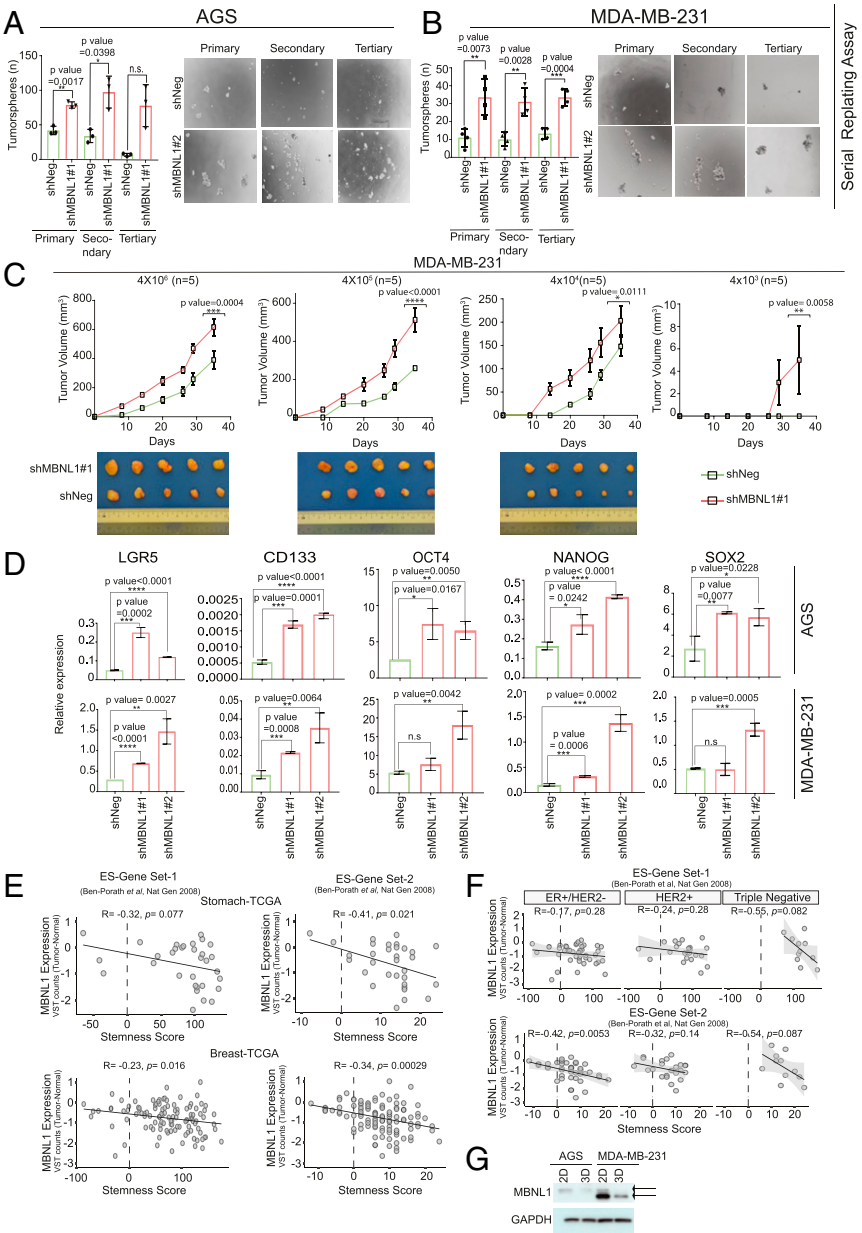

Fig. 4. MBNL1 down-regulation leads to increased stem/progenitor-like properties in cancer. (*A* and *B*) Bar graph (*Left*) and representative images at 10× magnification (*Right*) showing mean (±SD) number of tumorspheres formed by cells transfected with shNeg and shMBNL1#2 in primary, secondary, and tertiary plating for indicated cell lines ($n = 3$). (*C*) X-Y graph (*Top*) showing mean ± SD tumor volume (mm3) over time (days) in NOD/SCID mice s.c. injected with MDA-MB-231 cells treated with shNeg control shRNA (green) vs. MBNL1 KD cells (red) at indicated dilutions. (*Bottom*) Representative images of excised tumors. (*D*) Relative expression of *LGR5*, *CD133*, *OCT4*, *NANOG*, and *SOX2* in control and MBNL1 KD cells. Data show mean ± SD. (*E*) Scatterplot showing correlation between MBNL1 expression and stemness score in matched TCGA tumor/normal stomach and breast cancer samples. (*F*) Scatterplot showing correlation between MBNL1 expression and stemness score in three subtypes of breast adenocarcinoma. (*G*) Western blot showing MBNL1 expression in indicated cell lines grown either as monolayer or in suspension as tumor spheroids.

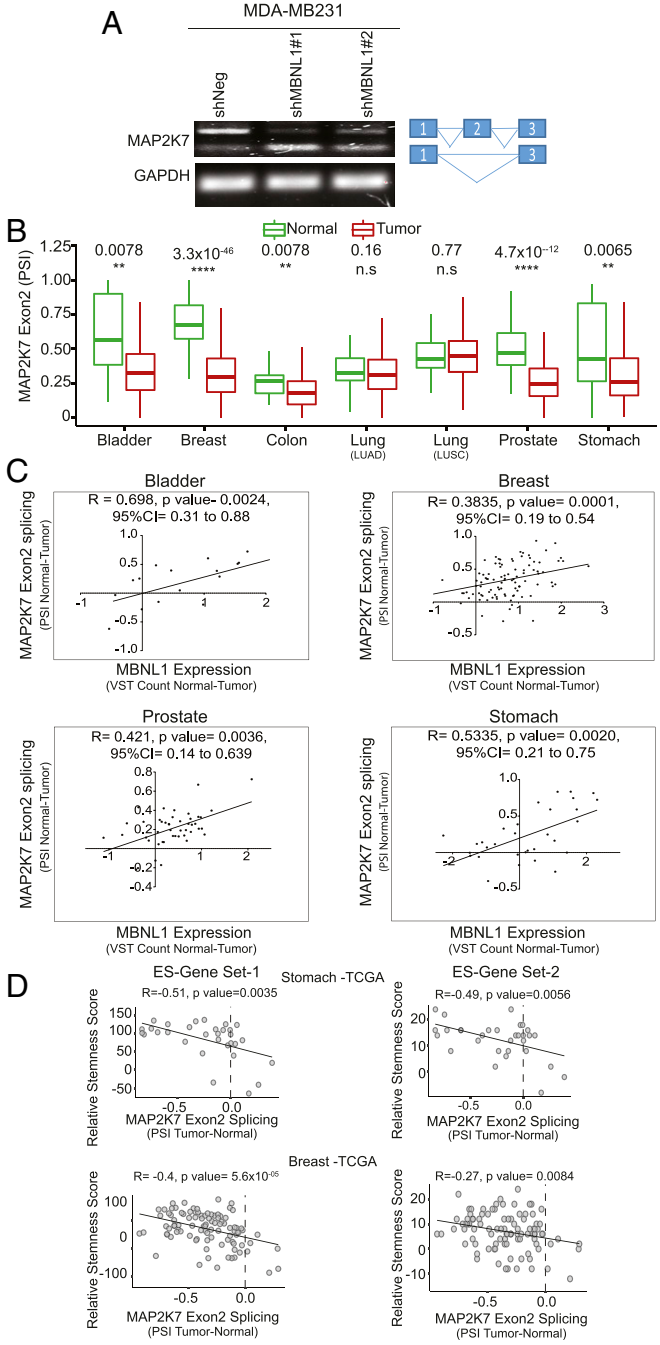

Fig. 5. MBNL1 regulates *MAP2K7* exon2 skipping. (*A*) RT-PCR validation of skipping of *MAP2K7* exon2 in the stable MBNL1 KD MDA-MB-231 cell line. (*B*) Box plots showing median PSI values for *MAP2K7* exon2 SIE in indicated cancer types using all available normal and tumor samples from TCGA. n.s. refers to not significant. (*C*) Scatterplots showing correlation between *MBNL1* mRNA expression and *MAP2K7* exon2 delta PSI values in matched tumor normal pairs in indicated cancer types. (*D*) Scatterplot showing correlation between stemness score and delta PSI value of *MAP2K7* exon2 of matched TCGA tumor and normal cancer samples.

failed to activate JNK upon serum stimulation despite showing low MBNL1 and high *MAP2K7*Δexon2 expression (Fig. 6*B*). We next scored TCGA patients for JNK activity gene expression signature (42) and correlated the expression of *MBNL1* and *MAP2K7* exon2 PSI to the JNK activity score (JAS). We found that *MBNL1* down-regulation as well as up-regulation of *MAP2K7*Δexon2 splice isoform is significantly correlated to increased JAS in breast cancer (*SI Appendix*, Fig. S6 *F* and *G*). Altogether, we conclude that *MBNL1* expression and *MAP2K7* exon2 splicing status are determinants for JNK pathway activation.

To directly examine the role of *MAP2K7*Δexon2 splice isoform in cellular dedifferentiation and cancer stem/progenitor-like properties, we used an antisense morpholino (AMO) directed against the 5′ splice site of *MAP2K7* exon2 (36) to force *MAP2K7* exon2 skipping in HFE-145 cells. This produced robust exon2 skipping and activation of JNK signaling (Fig. 6 *D* and *E*) as previously reported (36). Most importantly it drove up-regulation of CSC and pluripotency markers (CD133, NANOG, and SOX2, Fig. 6*F*) and increased trans-well migration and invasion (Fig. 6*G*), thereby recapitulating stemness phenotype observed upon loss of MBNL1 expression. Surprisingly, the MAP2K7 AMO also led to up-regulation of MAP2K7 and a modest (~30%) down-regulation of MBNL1 proteins, suggesting feedback signaling (Fig. 6 *E*, *Right*).

Next, we ectopically expressed a MAP2K7–JNK1 fusion construct in HFE-145 cells to assess whether activation of JNK signaling alone can recapitulate the MBNL1 down-regulation-mediated cancer stemness phenotype. As expected, this construct robustly activated JNK signaling (Fig. 6 *H*, *Left*), up-regulated CSC (*LGR5* and *CD133*) and pluripotency (*NANOG* and *SOX2*) markers (Fig. 6*I*), and increased migration and invasion (Fig. 6*J*). However, we failed to observe down-regulation of MBNL1 protein upon ectopic expression of the MAP2K7–JNK1 construct. In all, our data delineate a mechanism in which MBNL1 functions as a suppressor of stemness in cancer by preventing up-regulation of the *MAP2K7*Δexon2 isoform and JNK activation.

MBNL1-Low/*MAP2K7*Δexon2-High CSC-Like Cells Have Enhanced Susceptibility to JNK Inhibition. In our final set of experiments, we explored the potential of JNK inhibitors in reversing a MBNL1-low stem/progenitor-like phenotype. To this end, we used two small molecules (SP600125 [10 μM] and JNK-IN-8 [5 μM]) and a peptide inhibitor (D-JNKI-1, that is currently in phase III clinical trials for hearing loss and ocular inflammation) against JNK. Inhibition of JNK signaling by the small molecules as well as by the peptide resulted in a marked reversal of up-regulation of CSC and pluripotency markers in MBNL1 KD cells (Fig. 7 *A* and *B* and *SI Appendix*, Fig. S7). Finally, we treated our panel of MBNL1-low/*MAP2K7*Δexon2-high and MBNL1-high/*MAP2K7*Δexon2-low cancer cell lines with different concentrations of JNK-IN-8 and measured cell viability after 24 h (*SI Appendix*, Fig. S8). JNK-IN-8 showed a threefold lower mean effective dose 50 (ED_{50}) in MBNL1-low/*MAP2K7*Δexon2-high cell lines compared to the MBNL1-high/*MAP2K7*Δexon2-low cell lines (Fig. 7*C*). This indicates MBNL1-low/*MAP2K7*Δexon2-high cells have an enhanced susceptibility to JNK inhibition. Taken together, our data demonstrate that down-regulation of MBNL1 is associated with an increased stemness phenotype in cancer driven by high levels of the *MAP2K7*Δexon2 isoform and increased JNK signaling, and that JNK inhibition can reverse this phenotype. Our data point to the important conclusion that *MAP2K7* exon2 splicing status can potentially be used as a biomarker to prognosticate patients with cancer for JNK inhibition therapy as MBNL1-low *MAP2K7*Δexon2-high cells show enhanced susceptibility to JNK inhibition.

Discussion

Here we discovered a tumor cell dedifferentiation mechanism that can be reversed by JNK inhibition (Fig. 7*D*). Earlier therapeutic strategies that target CSC-specific cell surface markers are in various stages of clinical development (43), but it remains unclear whether these approaches will eventually become successful and hence the need for identification of additional therapeutic approaches. The role of JNK signaling in cancer and stemness is well established. JNK signaling is important in CSC self-renewal and maintenance in triple-negative breast cancer (44) and colon cancer

(38). In colon cancer, JNK-mediated c-JUN phosphorylation sequesters away the Mbd3/NuRD repressive complex from the *LGR5* promoter, causing its up-regulation (45). Although JNK activity is known to be context dependent (46), our findings suggest that inhibition of JNK can be a promising strategy to target CSCs in the clinic.

Though previous studies have established that *MBNL1* is down-regulated in some cancers, we here provide an extensive survey across 16 cancer types in matched tumor and normal samples to identify eight common *MBNL1*-low solid cancers. We also show down-regulation of MBNL1 protein in clinical samples and cancer cell lines. We establish that *MBNL1* down-regulation is associated with poor prognosis, relapse, and metastasis. We found that *MBNL1* was significantly up-regulated in three subtypes of renal cancer (kidney chromophobe, kidney renal clear cell carcinoma, and kidney renal papillary cell carcinoma), likely indicating kidney-specific difference in MBNL1 function and regulation. Furthermore, we show that reduced MBNL1 levels increase in vitro and in vivo tumorigenesis in breast and stomach cancer cell line models, and drive acquisition of stem cell-like functional and transcriptomic properties. In the context of T cell activation, Martinez et al. reported that exon2 skipping in JNK kinase *MAP2K7* exposes a JNK docking site, leading to increased

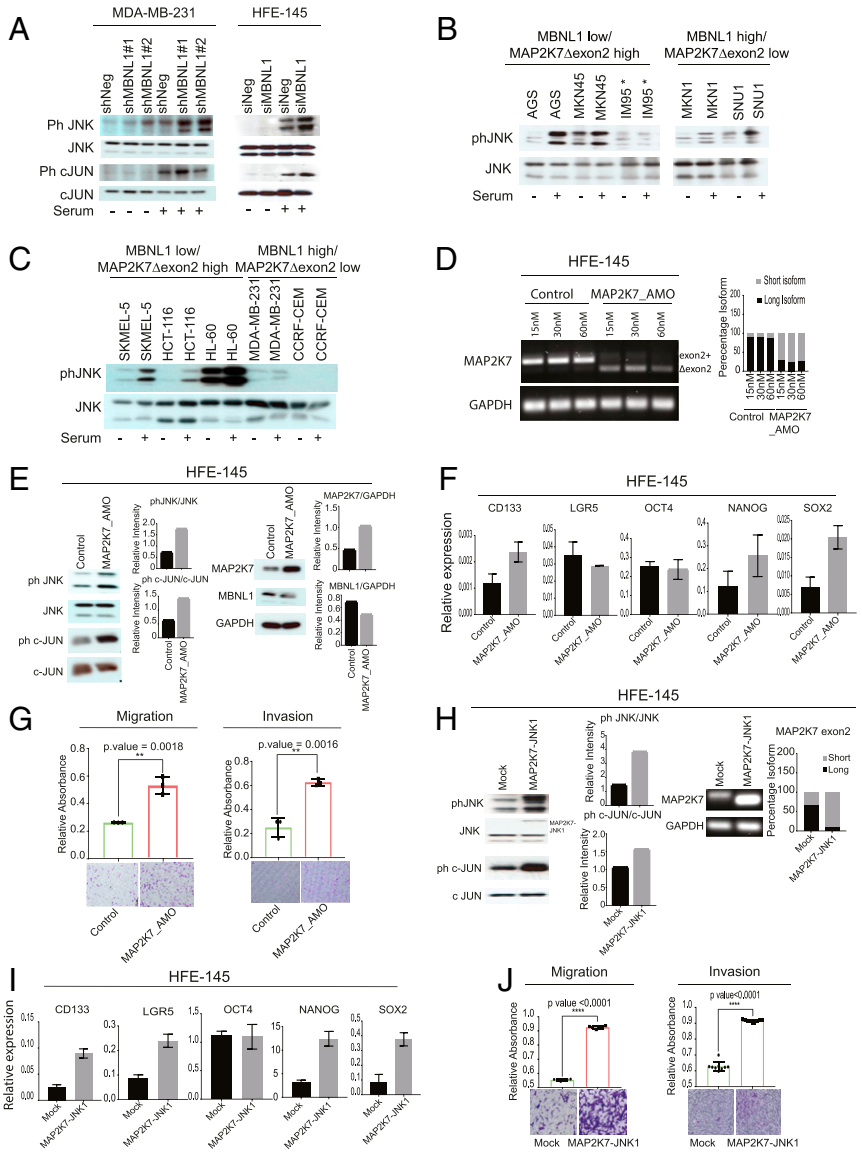

Fig. 6. Low levels of MBNL1 and consequent presence of *MAP2K7*Δexon2 splice form is associated with increased JNK signaling and acquisition of stem/progenitor-like properties. (*A*) Western blot analysis of ph-JNK, JNK, ph-c-JUN, and c-JUN in MBNL1 KD and control MDA-MB-231 and HFE-145 cells in the presence or absence of serum. (*B* and *C*) Western blot analysis of ph-JNK and JNK in a panel of MBNL1-low/*MAP2K7*Δexon2-high and MBNL1-high/*MAP2K7*Δexon2-low cell lines. Note for *B*, all protein lysates were analyzed on the same sodium dodecyl sulfate polyacrylamide gel but image was edited to exclude MKN7 due to technical reasons. This edit is indicated by visibly separating the image. (*D*) *MAP2K7* exon2 and *GAPDH* RT-PCR in HFE-145 cells transfected with control or *MAP2K7* exon2 AMO. (*E*) Western blot showing expression of ph-JNK, JNK, ph-c-JUN, c-JUN, MAP2K7, MBNL1, and GAPDH in HFE-145 cells treated with control or *MAP2K7* exon2 AMO. (*F* and *I*) qRT-PCR showing relative expression of *CD133*, *LGR5*, *OCT4*, *NANOG*, and *SOX2* in HFE-145 cells transfected with control or *MAP2K7* AMO and control or MAP2K7–JNK1 construct, respectively. Data show mean ± SD. (*G* and *J*) Bar graph (*Top*) and representative images (*Bottom*) showing migration (*Left*) and invasion (*Right*) in HFE-145 cells either transfected with control or *MAP2K7* AMO (*G*) and transfected with either control or MAP2K7–JNK1 construct (*J*). Data show mean ± SD. (*H*) Western blots of ph-JNK, JNK, ph-c-JUN, and c-JUN expression in HFE-145 cells mock transfected with vehicle alone or with 0.5 μg MAP2K7–JNK1 construct. *Right* shows semiquantitative RT-PCR of *MAP2K7* showing skipping of exon2 in HFE-145 cells transfected with MAP2K7–JNK1 construct.

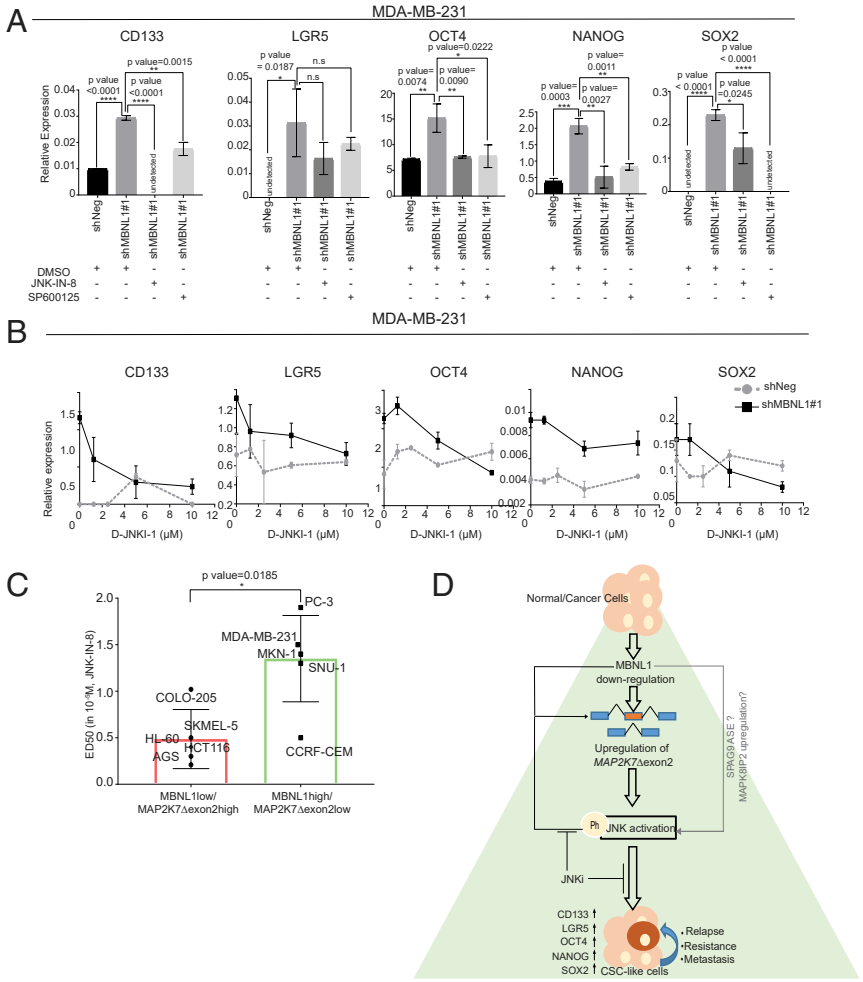

Fig. 7. JNK inhibition reverses MBNL1 KD-associated stem/progenitor-like properties. (*A* and *B*) qRT-PCR analysis showing mean (±SD) expression of *CD133*, *LGR5*, *OCT4*, *NANOG*, and *SOX2* relative to *GAPDH* in shNeg and shMBNL1 MDA-MB-231 cells treated either with dimethyl sulfoxide or with an indicated JNK inhibitor. (*C*) Bar plot showing mean of effective dose (ED_{50}) of MBNL1-low/MAP2K7Δexon2-high and MBNL1-lhigh/MAP2K7Δexon2-low cell lines treated with JNK-IN-8. (*D*) Graphical representation of the role and function of MBNL1–*MAP2K7*Δexon2–JNK signaling in cancer.

JNK activation (36). Our work extends from these findings by demonstrating that this is likely an ASE shared across many or all *MBNL1*-low cancers which largely drives the MBNL1 down-regulation-mediated tumor dedifferentiation that can be reversed by JNK inhibition. We speculate that other MBNL1-regulated ASEs, such as that in *SPAG9* and dysregulated expression of MAP kinase-related genes (e.g., up-regulation of *MAPK8IP2* that encodes the JNK interacting protein 2 or JIP2) associated with MBNL1 down-regulation feeds forward to activate JNK signaling and contributes to cancer stemness (Fig. 7*D*). Therefore, *MAP2K7*Δexon2 isoform joins a select few of cancer-associated splice events with a defined function in cancer.

Previous work suggested that JNK inhibition can effectivity target CSC populations (47). We here identify biomarkers that explain the molecular context by which some but not other forms of cancer would be candidates for JNK inhibition, possibly in combination with chemotherapy or immunotherapy to achieve relapse-free durable responses. D-JNKI-1 (XG-102) is the most promising JNK inhibitor currently in phase III clinical trials for hearing loss and ocular inflammation (48). D-JNKI-1 has also shown encouraging effects against tumor growth in a mouse skin cancer model (49). Our data show that D-JNKI-1 in vitro successfully reverses up-regulation of CSC and pluripotency markers in a *MBNL1*-low breast cancer cell line model. Accordingly, JNK-IN-8, which binds JNK1 irreversibly as a covalent adduct to the conserved cysteine[116] residue, consistently showed higher efficacy in MBNL1-low/*MAP2K7*Δexon2-high cancer cells. *MBNL1* and *MAP2K7*Δexon2 expression status, therefore, may function as effective biomarkers for predicting responsiveness to JNK inhibitors.

In conclusion, we show that MBNL1 is a prognostic marker, the loss of expression of which segregates with reduced overall survival. We reveal that MBNL1 down-regulation drives cancer cell dedifferentiation via a *MAP2K7*Δexon2–JNK signaling pathway. Our work identifies MBNL1 and MAP2K7Δexon2 as biomarkers that can be used to prognosticate patients for JNK inhibition therapy.

Materials and Methods

All cell lines used were exempted by the Institutional Review Board of the National University of Singapore following submission for review. Primary human stomach cancer and adjacent tissue samples were collected with informed consent of patients undergoing surgery by the Singapore tissue repository under the guidelines and policies of the SingHealth Centralized Institution Review Board. All procedures performed on mice were approved by the The Institutional Animal Care and Use Committee, Biological Resource Centre, A-Star, Singapore.

RNA-Sequencing Analysis to Measure Differential Splicing and Gene Expression. siNeg (two biological replicates) and siMBNL1 (three biological replicates) HFE-145 cells were used for RNA sequencing to generate 100 million paired-end reads. Reads were aligned to hg19 reference genome using STAR

aligner v2.4.2a (50). Exon-centric alternative splicing analysis was performed using MISO (27) to quantify relative abundance of alternative splice isoforms by a percent spliced in (PSI) value. We then performed pairwise comparison for all six pairs (two siNeg vs. three siMBNL1 samples). ASEs that have a ΔPSI (PSI_N-PSI_T) value >0.2 or < −0.2 in at least four out of the six pairs analyzed were defined as high-confidence ASEs. We further used the same dataset to analyze differential gene expression using DESeq2 (51). We considered genes with log2 fold change >0.5 and < −0.5 with an adjusted *P* value of <0.05 (Benjamini–Hochberg correction) to be differentially expressed.

See *SI Appendix* for *SI Appendix, Supplementary Materials and Methods* and Dataset S1, Tables S10 and S11 for primer sequences and reagents.

Data Availability. All RNA-seq data generated are available via European Nucleotide Archive (ENA) under accession no. PRJEB32567.

ACKNOWLEDGMENTS. We thank Prof. David Virshup for discussion and comments on the manuscript; Prof. Kanaga Sabapathy for providing the MAP2K7–JNK1 construct; Duke-NUS Genome Biology Facility, Duke-NUS, Singapore, for performing RNA sequencing; SingHealth Advanced Molecular Pathology Laboratory, Singapore, for IHC experiments; Dr. Manikandan Lakshmanan and Mr. Anandhkumar Raju from Institute of Molecular & Cell Biology, Singapore, for xenograft experiments; and Life Science Editors for scientific editing. This work was supported by the National Medical Research Council, Singapore (NMRC/OFYIRG/0065/2017 to D.R. and NMRC/CBRG/0104/2016 to D.M.E.).

1. F. E. Baralle, J. Giudice, Alternative splicing as a regulator of development and tissue identity. *Nat. Rev. Mol. Cell Biol.* **18**, 437–451 (2017).
2. E. T. Wang *et al.*, Alternative isoform regulation in human tissue transcriptomes. *Nature* **456**, 470–476 (2008).
3. C. J. David, J. L. Manley, Alternative pre-mRNA splicing regulation in cancer: Pathways and programs unhinged. *Genes Dev.* **24**, 2343–2364 (2010).
4. S. Oltean, D. O. Bates, Hallmarks of alternative splicing in cancer. *Oncogene* **33**, 5311–5318 (2014).
5. H. Zhang *et al.*, CD44 splice isoform switching determines breast cancer stem cell state. *Genes Dev.* **33**, 166–179 (2019).
6. H. L. Goel *et al.*, Regulated splicing of the α6 integrin cytoplasmic domain determines the fate of breast cancer stem cells. *Cell Rep.* **7**, 747–761 (2014).
7. Y. Ge *et al.*, Alternative splice variants of DCLK1 mark cancer stem cells, promote self-renewal and drug-resistance, and can be targeted to inhibit tumorigenesis in kidney cancer. *Int. J. Cancer* **143**, 1162–1175 (2018).
8. Y. Miao *et al.*, Adaptive immune resistance emerges from tumor-initiating stem cells. *Cell* **177**, 1172–1186.e14 (2019).
9. D. Friedmann-Morvinski, I. M. Verma, Dedifferentiation and reprogramming: Origins of cancer stem cells. *EMBO Rep.* **15**, 244–253 (2014).
10. N. Salomonis *et al.*, Alternative splicing in the differentiation of human embryonic stem cells into cardiac precursors. *PLoS Comput. Biol.* **5**, e1000553 (2009).
11. M. Gabut *et al.*, An alternative splicing switch regulates embryonic stem cell pluripotency and reprogramming. *Cell* **147**, 132–146 (2011).
12. H. Han *et al.*, MBNL proteins repress ES-cell-specific alternative splicing and reprogramming. *Nature* **498**, 241–245 (2013).
13. P. Konieczny, E. Stepniak-Konieczna, K. Sobczak, MBNL proteins and their target RNAs, interaction and splicing regulation. *Nucleic Acids Res.* **42**, 10873–10887 (2014).
14. A. Masuda *et al.*, CUGBP1 and MBNL1 preferentially bind to 3′ UTRs and facilitate mRNA decay. *Sci. Rep.* **2**, 209 (2012).
15. R. Batra *et al.*, Loss of MBNL leads to disruption of developmentally regulated alternative polyadenylation in RNA-mediated disease. *Mol. Cell* **56**, 311–322 (2014).
16. E. T. Wang *et al.*, Dysregulation of mRNA localization and translation in genetic disease. *J. Neurosci.* **36**, 11418–11426 (2016).
17. T. Tabaglio *et al.*, MBNL1 alternative splicing isoforms play opposing roles in cancer. *Life Sci. Alliance* **1**, e201800157 (2018).
18. L. Fish *et al.*, Muscleblind-like 1 suppresses breast cancer metastatic colonization and stabilizes metastasis suppressor transcripts. *Genes Dev.* **30**, 386–398 (2016).
19. L. Tang, P. Zhao, D. Kong, Muscleblind-like 1 destabilizes Snail mRNA and suppresses the metastasis of colorectal cancer cells via the Snail/E-cadherin axis. *Int. J. Oncol.* **54**, 955–965 (2019).
20. E. Sebestyén *et al.*, Large-scale analysis of genome and transcriptome alterations in multiple tumors unveils novel cancer-relevant splicing networks. *Genome Res.* **26**, 732–744 (2016).
21. K. Y. Lee *et al.*, Compound loss of muscleblind-like function in myotonic dystrophy. *EMBO Mol. Med.* **5**, 1887–1900 (2013).
22. H. Tran *et al.*, Analysis of exonic regions involved in nuclear localization, splicing activity, and dimerization of Muscleblind-like-1 isoforms. *J. Biol. Chem.* **286**, 16435–16446 (2011).
23. M. Danan-Gotthold *et al.*, Identification of recurrent regulated alternative splicing events across human solid tumors. *Nucleic Acids Res.* **43**, 5130–5144 (2015).
24. D. P. Gates, L. A. Coonrod, J. A. Berglund, Autoregulated splicing of muscleblind-like 1 (MBNL1) Pre-mRNA. *J. Biol. Chem.* **286**, 34224–34233 (2011).
25. C. Curtis *et al.*; METABRIC Group, The genomic and transcriptomic architecture of 2,000 breast tumours reveals novel subgroups. *Nature* **486**, 346–352 (2012).
26. A. Forero *et al.*, Expression of the MHC class II pathway in triple-negative breast cancer tumor cells is associated with a good prognosis and infiltrating lymphocytes. *Cancer Immunol. Res.* **4**, 390–399 (2016).
27. Y. Katz, E. T. Wang, E. M. Airoldi, C. B. Burge, Analysis and design of RNA sequencing experiments for identifying isoform regulation. *Nat. Methods* **7**, 1009–1015 (2010).
28. S. Cheng *et al.*, A functional network of gastric-cancer-associated splicing events controlled by dysregulated splicing factors. *NAR Genom. Bioinform.* **2**, lqaa013 (2020).
29. E. G. Bechara, E. Sebestyén, I. Bernardis, E. Eyras, J. Valcárcel, RBM5, 6, and 10 differentially regulate NUMB alternative splicing to control cancer cell proliferation. *Mol. Cell* **52**, 720–733 (2013).
30. Z. Wang, G. Ouyang, Periostin: A bridge between cancer stem cells and their metastatic niche. *Cell Stem Cell* **10**, 111–112 (2012).
31. M. Sakaki-Yumoto, Y. Katsuno, R. Derynck, TGF-β family signaling in stem cells. *Biochim. Biophys. Acta* **1830**, 2280–2296 (2013).
32. H. Shen *et al.*, Sox4 expression confers bladder cancer stem cell properties and predicts for poor patient outcome. *Int. J. Biol. Sci.* **11**, 1363–1375 (2015).
33. I. Ben-Porath *et al.*, An embryonic stem cell-like gene expression signature in poorly differentiated aggressive human tumors. *Nat. Genet.* **40**, 499–507 (2008).
34. L. Cao *et al.*, Sphere-forming cell subpopulations with cancer stem cell properties in human hepatoma cell lines. *BMC Gastroenterol.* **11**, 71 (2011).
35. D. T. Ho, A. J. Bardwell, S. Grewal, C. Iverson, L. Bardwell, Interacting JNK-docking sites in MKK7 promote binding and activation of JNK mitogen-activated protein kinases. *J. Biol. Chem.* **281**, 13169–13179 (2006).
36. N. M. Martinez *et al.*, Widespread JNK-dependent alternative splicing induces a positive feedback loop through CELF2-mediated regulation of MKK7 during T-cell activation. *Genes Dev.* **29**, 2054–2066 (2015).
37. F. Chen, JNK-induced apoptosis, compensatory growth, and cancer stem cells. *Cancer Res.* **72**, 379–386 (2012).
38. M. Fang *et al.*, IL33 promotes colon cancer cell stemness via JNK activation and macrophage recruitment. *Cancer Res.* **77**, 2735–2745 (2017).
39. M. Akerman, H. David-Eden, R. Y. Pinter, Y. Mandel-Gutfreund, A computational approach for genome-wide mapping of splicing factor binding sites. *Genome Biol.* **10**, R30 (2009).
40. M. B. Warf, J. A. Berglund, MBNL binds similar RNA structures in the CUG repeats of myotonic dystrophy and its pre-mRNA substrate cardiac troponin T. *RNA* **13**, 2238–2251 (2007).
41. A. M. Hudson *et al.*, Truncation- and motif-based pan-cancer analysis reveals tumor-suppressing kinases. *Sci. Signal.* **11**, eaan6776 (2018).
42. M. Ashenden *et al.*, An *in vivo* functional screen identifies JNK signaling as a modulator of chemotherapeutic response in breast cancer. *Mol. Cancer Ther.* **16**, 1967–1978 (2017).
43. K. Chen, Y. H. Huang, J. L. Chen, Understanding and targeting cancer stem cells: Therapeutic implications and challenges. *Acta Pharmacol. Sin.* **34**, 732–740 (2013).
44. X. Xie *et al.*, c-Jun N-terminal kinase promotes stem cell phenotype in triple-negative breast cancer through upregulation of Notch1 via activation of c-Jun. *Oncogene* **36**, 2599–2608 (2017).
45. C. Aguilera *et al.*, c-Jun N-terminal phosphorylation antagonises recruitment of the Mbd3/NuRD repressor complex. *Nature* **469**, 231–235 (2011).
46. C. Tournier, The 2 faces of JNK signaling in cancer. *Genes Cancer* **4**, 397–400 (2013).
47. C. Kitanaka, A. Sato, M. Okada, JNK signaling in the control of the tumor-initiating capacity associated with cancer stem cells. *Genes Cancer* **4**, 388–396 (2013).
48. J. Cicenas, JNK inhibitors: Is there a future. *MAP Kinase* **4**, 5700 (2015).
49. Y. J. Gao *et al.*, Selective inhibition of JNK with a peptide inhibitor attenuates pain hypersensitivity and tumor growth in a mouse skin cancer pain model. *Exp. Neurol.* **219**, 146–155 (2009).
50. A. Dobin *et al.*, STAR: Ultrafast universal RNA-seq aligner. *Bioinformatics* **29**, 15–21 (2013).
51. M. I. Love, W. Huber, S. Anders, Moderated estimation of fold change and dispersion for RNA-seq data with DESeq2. *Genome Biol.* **15**, 550 (2014).